

# Towards inference of human brain connectivity from MR diffusion tensor data

C. Poupon<sup>a,b,\*</sup>, J.-F. Mangin<sup>a</sup>, C.A. Clark<sup>a</sup>, V. Frouin<sup>a</sup>, J. Régis<sup>c</sup>, D. Le Bihan<sup>a</sup>, I. Bloch<sup>b</sup>

<sup>a</sup>*Service Hospitalier Frédéric Joliot, CEA, 4 Place du Général Leclerc, 91401 Orsay Cedex, France*

<sup>b</sup>*Département Signal et Image, ENST, Paris, France*

<sup>c</sup>*Service de Neurochirurgie Fonctionnelle et Stéréotaxique, CHU, La Timone, France*

Received 25 November 1999; accepted 27 July 2000

## Abstract

This paper describes a method to infer the connectivity induced by white matter fibers in the living human brain. This method stems from magnetic resonance tensor imaging (DTI), a technique which gives access to fiber orientations. Given typical DTI spatial resolution, connectivity is addressed at the level of fascicles made up by a bunch of parallel fibers. We propose first an algorithm dedicated to fascicle tracking in a direction map inferred from diffusion data. This algorithm takes into account fan-shaped fascicle forks usual in actual white matter organization. Then, we propose a method of inferring a regularized direction map from diffusion data in order to improve the robustness of the tracking. The regularization stems from an analogy between white matter organization and spaghetti plates. Finally, we propose a study of the tracking behavior according to the weight given to the regularization and some examples of the tracking results with in vivo human brain data. © 2001 Elsevier Science B.V. All rights reserved.

*Keywords:* Diffusion, Connectivity, White matter, Bundle, Regularization

## 1. Introduction

During the last decade, the development of magnetic resonance imaging (MRI) has led to the design of numerous segmentation methods dedicated to brain structures. For instance, cortex, white matter and basal ganglia can be extracted from standard T1-weighted MR images (Mangin et al., 1995; Poupon et al., 1998b). While such structures can be identified from a priori knowledge on MR signal and simple anatomical considerations, further brain parcellations are much more difficult to perform from macroscopic images.

However, discussions concerning the nature of psychological phenomena and their neurobiological bases often make reference to networks of brain areas. For instance, the thalamus is made up of numerous elementary nuclei;

the cortical sheet can be divided in areas according to various maps related to architectural features. Moreover, information about forward and backward connections between these elementary areas has been inferred from invasive anatomical techniques for several animal species (Young et al., 1995). While a number of objections can be raised against these oversimplified architectural models, they have provided invaluable reference systems for neuroscience studies. Indeed, these parcellations and their connectivity are considered to be reproducible between individuals of the same species and share important similarities across species.

Unfortunately, most of the architectural information underlying these reference systems cannot be accessed in the living human brain. Therefore, the neuroimaging community has designed its own reference system in a very different way. This system, inspired from Talairach proportional system for surgery planning (Talairach et al., 1967), simply relies on 3D coordinates indicating a location in a template brain. Each new brain is endowed

\*Corresponding author. Tel.: +33-1-6986-7813; fax: +33-1-6986-7868.

E-mail address: cpoupon@shfj.cea.fr (C. Poupon).

with this coordinate system through spatial normalization, namely a 3D deformation matching as far as possible the new brain macroscopic anatomy with that of the template. While spatial normalization is often required to compare functional images across individuals and across experiments (Fox et al., 1985), no simple link between the proportional system and usual architectural parcellations can be provided apart from a statistical one (Roland and Zilles, 1994).

Although impressive refinements of the normalization scheme have been achieved by the image analysis community during the last years (Miller et al., 1993; Thirion, 1998), most of these developments are bound to drift towards pure morphing approaches without consistent architectural justification. Indeed, considering the absence of a gold standard, more attention should be given to architectural value of the different features used to drive the deformation processes. In fact nobody really knows today how brains should be matched. Furthermore, nobody knows to which extent matching two different brains with a continuous deformation makes sense from a neuroscience point of view.

A first approach to increasing the role of brain architecture in spatial normalization procedures consists in imposing the perfect matching of a few well-known cortical folds (Thompson et al., 1996; Lohman and Von Cramon, 1998). Indeed, the largest cortical fissures are endowed with clear architectural value. Unfortunately, extending this approach to a higher number of folds requires better understanding of the inter-individual variability of the folding patterns (Régis et al., 1995). Furthermore, the putative architectural value of secondary folds has still to be proven.

While an increasing number of studies are dedicated to the cortex folding patterns, few groups try to analyse the complex shape of white matter (Mangin et al., 1996; Naf et al., 1996). Indeed, standard imaging modalities give little information on the underlying bundle entanglement. In this paper, we describe an emerging MR technique which may radically modify the situation. Indeed, this technique called diffusion tensor imaging (DTI), gives access to the macroscopic organization of brain white matter (Le Bihan, 1995). The basic principle stems from the orientational information provided by the phenomenon of water diffusion anisotropy in white matter. Diffusion tensor imaging characterises the diffusional behaviour of water in tissue on a voxel by voxel basis. For each voxel, the diffusion tensor yields the diffusion coefficient corresponding to any direction in space (Basser et al., 1994b). Given that one may ascribe diffusion anisotropy in white matter to a greater hindrance or restriction to diffusion across fiber axes than along them, the direction corresponding to the highest diffusion coefficient may be considered to point along a putative fiber bundle traversing the voxel. Thus, maps of the highest diffusion direction can be produced which provide a striking visualization of the white matter pathways and their orientation.

This paper addresses the reconstruction of fiber trajectories from such direction maps. The general aim is the mapping of structural connectivity, that is, the possibility to assert which cortical areas or basal ganglia are connected by fascicles embedded in white matter bundles. This would allow the neuroimaging community to bring its methodology closer to the ones used in standard neuroscience. Furthermore, this would allow the improvement of current models of the human cortex connectivity. Indeed, up to now, tract tracing methodologies dedicated to the human brain have been restricted to post mortem methods, which are not competitive compared with invasive methods used for animals (Young et al., 1995).

The possibility to track the putative trajectories of some fascicles, namely small fiber bundles, has been convincingly proven by several recent studies (Poupon et al., 1998a; Conturo et al., 1999; Mori et al., 1999). However, the robustness of methods which simply consist in following the direction of highest diffusion in a step by step fashion may be discussed with regard to low spatial resolution and artefacts inherent to *in vivo* MR diffusion data. In this paper, we address the ill-posed nature of the problem which in our opinion calls for a regularization framework.

The paper is organized as follows. In the first section, the various stages of the process leading to the computation of tensor images from a sequence of diffusion-weighted data are briefly delineated. The second section outlines a simple fascicle tracking algorithm dealing with potential junctions between fascicles. This algorithm converts any direction map extracted from diffusion data into a tracking map. The third section highlights the ill-posed nature of the tracking problem which calls for a regularization framework. This need lead us to design Markovian models aimed at modeling the geometry of white matter which is compared to the geometry of spaghetti plates. Then, one of these models is used as a priori knowledge to infer a regularized direction map from raw tensor diffusion data. In a final section, we study the tracking algorithm behaviour according to the regularization weight and describe some tracking results obtained in a series of normal volunteers.

## 2. Diffusion tensor images

In brain tissues, molecules are endowed with a Brownian motion macroscopically leading to a diffusion process (Le Bihan, 1995). In the case of isotropic liquids, the probability that a molecule covers distance  $r$  during time  $t$  follows a Gaussian law with variance  $6ct$  where  $c$  is the diffusion coefficient that characterizes molecule mobility. In anisotropic environments, mobility is different along each direction of space. Hence, diffusion is a tridimensional process which can be modeled by a second-order tensor. This tensor is represented by a matrix  $[T]$  which is symmetric, positive and real. The diffusion coefficient in

any direction  $\vec{d}$  is given by the tensorial dot product (Eq. 1).  $[T]$  is an intrinsic property of the tissue.

$$c(\vec{d}) = \vec{d} \cdot [T] \vec{d}, \quad \text{with } [T] = \begin{pmatrix} T_{xx} & T_{xy} & T_{xz} \\ T_{xy} & T_{yy} & T_{yz} \\ T_{xz} & T_{yz} & T_{zz} \end{pmatrix}. \quad (1)$$

The MR signal is usually corrupted by water molecule diffusion which disturbs spin echo techniques leading to a small decrease of the measured signal. In diffusion imaging, this effect is magnified by a large gradient applied in one direction  $\vec{d}$ . When the diffusion process is included in the equations modeling MR phenomena, the signal decay turns out to be exponentially related to the diffusion coefficient  $c(\vec{d})$  in the gradient direction multiplied by a ‘ $b$  factor’ related to gradient amplitude. Hence, acquisition of several diffusion-weighted images from a set of different gradient amplitudes allows the estimation of  $c(\vec{d})$ . When the diffusion process is anisotropic, the use of at least six gradient directions allows the estimation of the tensor matrix (Basser et al., 1994b).

### 2.1. Data acquisition

All scans were acquired on a 1.5T Signa Horizon Echospeed MRI system (Signa, General Electric Medical Systems, Milwaukee, USA) equipped with magnetic field gradients of up to 22 mT/m. A standard quadrature head coil was used for RF transmission and reception of the NMR signal. Head motion was minimised with standard foam padding as provided by the manufacturer.

The following images were acquired after a sagittal

localiser scan. An inversion recovery prepared spoiled gradient echo sequence was used to obtain a high resolution T1-weighted anatomical image of the whole brain ( $1.0 \times 1.0 \times 1.3$  mm resolution). Echo-planar diffusion-weighted images were acquired in the axial plane. Blocks of eight contiguous slices were acquired each 2.8 mm thick. Seven blocks were acquired covering the entire brain corresponding to 56 slice locations. For each slice location 31 images were acquired; a T2-weighted image with no diffusion sensitization followed by five diffusion sensitized sets ( $b$  values linearly incremented to a maximum value of  $1000 \text{ s/mm}^2$ ) in each of six non-collinear directions. These directions were as follows:  $\{(1,1,0), (1,0,1), (0,1,1), (1,-1,0), (1,0,-1), (0,1,-1)\}$  providing the best precision in the tensor component when six directions are used (Basser and Pierpaoli, 1998). In order to improve the SNR this was repeated four times, providing 124 images per slice location. The image resolution was  $128 \times 128$ , field of view  $24 \times 24$  cm, TE = 84.4 ms, TR = 2.5 s. Imaging time excluding time for on-line reconstruction was approximately 37 minutes. A database of eight normal volunteers (men, age range 25–34 years) has been acquired with this protocol. All subjects gave informed consent and the study was approved by the local Ethics Committee.

### 2.2. Distortion correction

Before performing the tensor estimation, a correction algorithm is applied to the diffusion-weighted dataset to correct for distortions related to eddy currents induced by the large diffusion gradients. Indeed, distortion amplitude reaches 1 cm for the highest gradients which prevents a

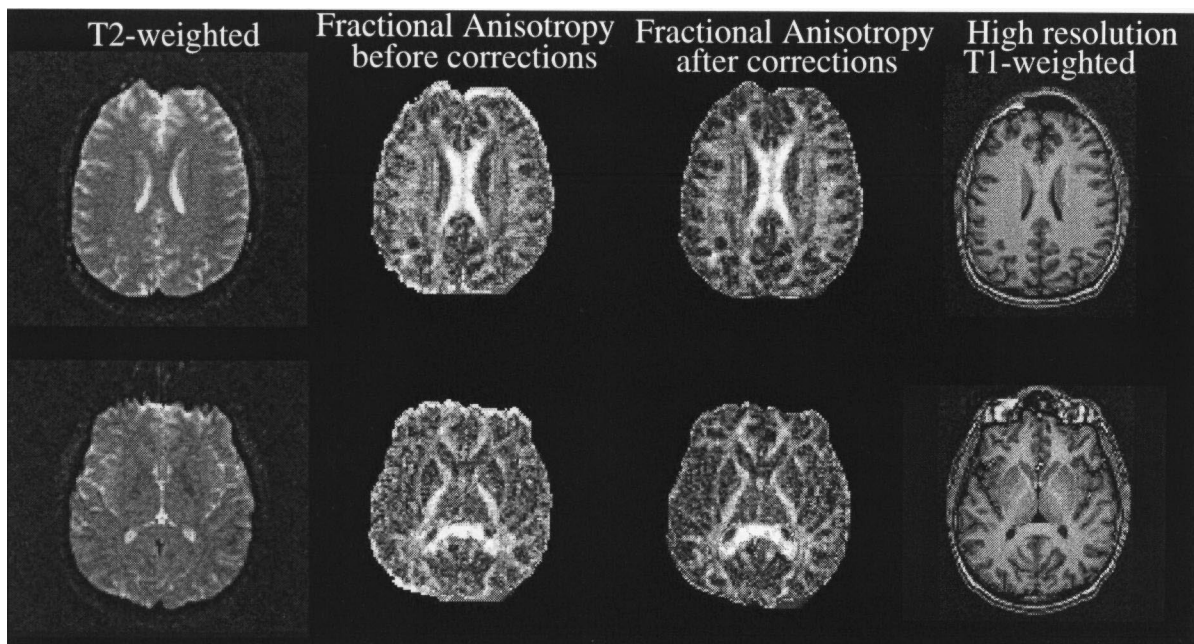


Fig. 1. Correction for the spatial distortions induced by eddy currents and computation of diffusion tensor using a robust regression method highly improve anisotropy maps.

consistent tensor matrix estimation. The correction algorithm relies on a three-parameter distortion model including scale, shear and linear translation in the phase-encoding direction (Haselgrove and Moore, 1996). The optimal parameters are assessed independently for each slice relative to the T2-weighted corresponding image using mutual information maximization (Wells et al., 1997). The improvements induced by this correction are illustrated by Fig. 1 using maps made up of a measure of tensor

anisotropy (Basser and Pierpaoli, 1996). In such maps, white matter high anisotropy is clearly contrasted with surrounding gray matter and cerebrospinal fluid areas.

Distortion correction removes border artefacts and improves spatial resolution.

### 2.3. Robust regression

The six coefficients of the tensor symmetric matrix are

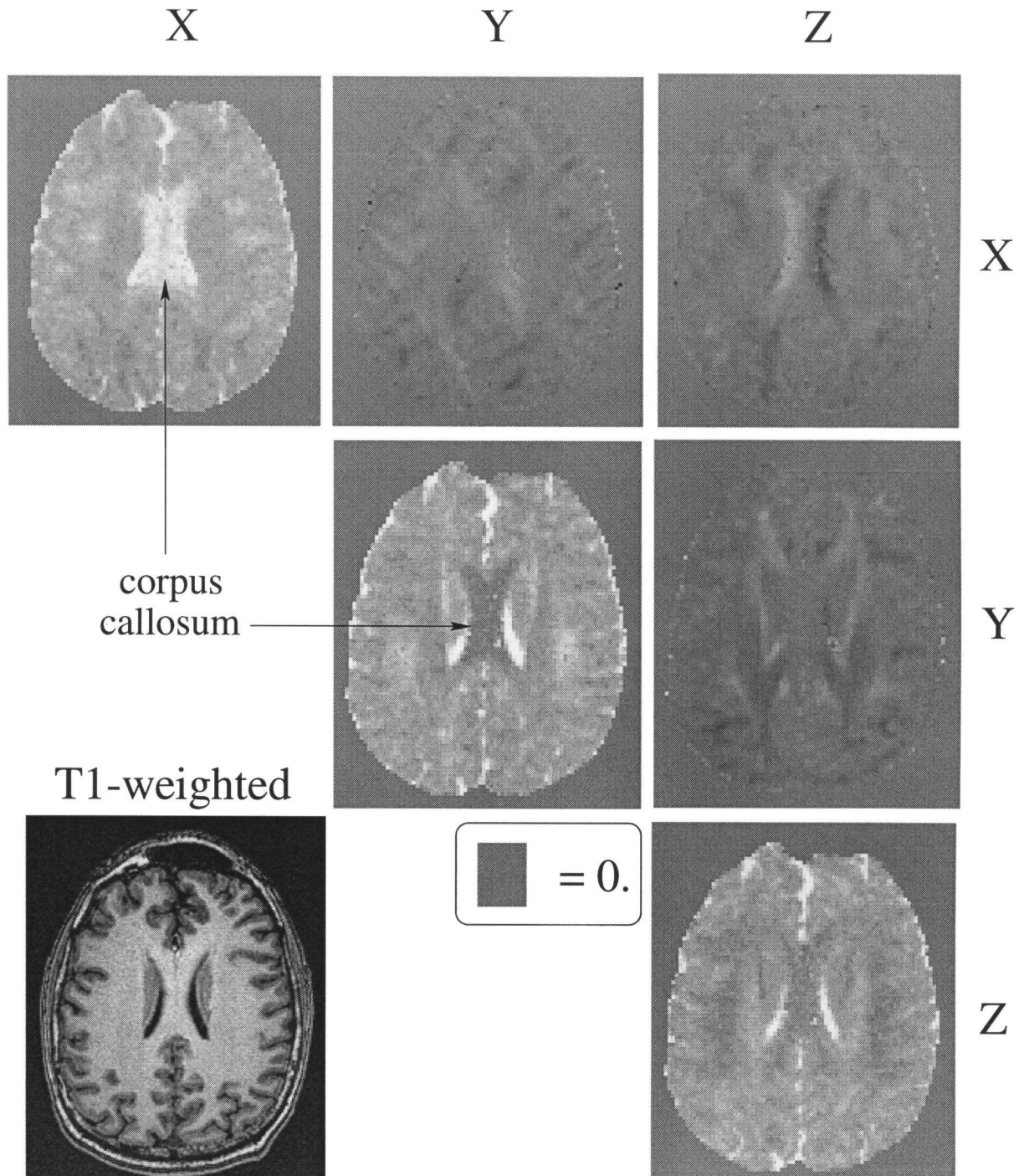


Fig. 2. A slice of a diffusion tensor volume.

usually calculated for each voxel of the brain using a mean square estimator (Basser et al., 1994a). However, diffusion-weighted data are often corrupted by artefacts related to physiological motions (cardiac cycle, etc.) which may bias these kind of estimators. Therefore we use a robust regression method which belongs to the M-estimator family (Meer et al., 1991). This method may be regarded as an iterated weighted least-squares which discards outliers. Such methods remain reliable as long as less than half of the data are contaminated by outliers. A detailed description of this tensor reconstruction process is beyond the scope of this paper. An example of one tensor image is shown in Fig. 2.

### 3. Computation of the tracking map

This section outlines a method which transforms any direction map inferred from diffusion data into a tracking map. A direction map is an image of unitary vectors which indicate the putative local fiber directions. Usually, such direction maps are simply made up of the tensor eigenvector associated with the highest eigenvalue. In the following, we will propose a method to construct regularized direction maps according to a priori knowledge on white matter geometry. A tracking map endows each voxel of white matter with a way of tracking forwards or backwards the fascicle crossing this voxel. Some voxels of the map which represent forks may split the tracking process into several trajectories (cf. Fig. 3). Brain connectivity inference amounts to converting an input area into an output area through the tracking possibilities provided by the tracking map.

#### 3.1. White matter mask

The initial stage of the tracking approach consists in defining a segmented mask  $\mathcal{W}$  on which will be restricted all the methods described in the following. This mask, which is made up of the voxels belonging to white matter, is automatically extracted from the T1-weighted image using an algorithm developed in our institution (Mangin et

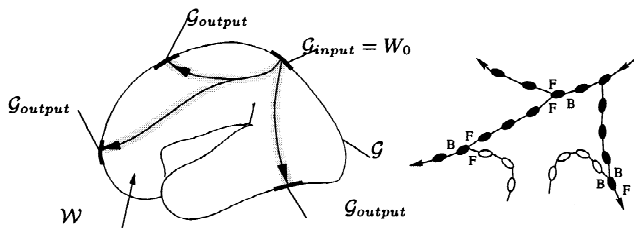


Fig. 3. Tracking process: the tracking starts at a subset  $\mathcal{G}_{input}$  of the boundary  $\mathcal{G}$  between white and gray matter; it uses  $\mathcal{F}(M)$  and  $\mathcal{B}(M)$  linked neighbor sets to propagate through white matter until a cortical or basal  $\mathcal{G}_{output}$  region is reached. The behaviour of the tracking algorithm at the level of forks is illustrated on the right.

al., 1995, 1998). A morphological homotopic dilation is then applied to this segmentation in order to be robust to potential distortions between the echo-planar images (DTI) and the high resolution T1-weighted image. The homotopic constraint prevents the filling in of cortical folds, which may lead to absurd tracking trajectories.

#### 3.2. Best neighbors

Let  $\vec{d}(M)$  denote the direction associated with voxel  $M \in \mathcal{W}$ . Since fascicles cannot end up inside white matter, we have to find forwards and backwards relative to  $\vec{d}(M)$  either  $\mathcal{W}$  boundary or at least one neighboring voxel associated with a compatible local fiber direction. Here, compatibility stems from the a priori hypothesis that most of the white matter fascicles are endowed with slow direction variations. This subsection describes a linking rule which defines the best forward and backward neighbor of each voxel. This rule is related to the topology proposed by Jones et al. (1999) to define major bundles as connected components. Nevertheless, Jones et al.'s linking rule is too tolerant to deal with brain connectivity because a bunch of bundles that cross the same white matter bottleneck (corpus callosum, internal capsule) belong to the same connected component. The notion of best neighbor allows us to split large bundles into fascicle sets.

Each voxel  $M$  is endowed with a forward and a backward conic neighborhood  $\mathcal{N}_f^\beta(M)$  and  $\mathcal{N}_b^\beta(M)$  defined from  $\vec{d}(M)$  (see Fig. 4). The conic neighborhood  $\mathcal{N}_f^\beta(M)$  (respectively  $\mathcal{N}_b^\beta(M)$ ) is defined as the subset of the 26-neighbors of  $M$  belonging to the half-cone whose apex is  $M$ , whose direction is  $\vec{d}(M)$  (respectively  $-\vec{d}(M)$ ) and whose aperture angle is  $\beta$  (typically set to  $45^\circ$ ).

In this subsection, a voxel  $M$  can be linked to at most one voxel  $f(M)$  (respectively  $b(M)$ ) of  $\mathcal{N}_f^\beta(M)$  (respectively  $\mathcal{N}_b^\beta(M)$ ). The linked forward neighbor  $f(M)$  is defined if the set  $\mathcal{N}_{fs}^\beta(M) = \{P \in \mathcal{N}_f^\beta(M), M \in \mathcal{N}_f^\beta(P) \cup \mathcal{N}_b^\beta(P)\}$  is

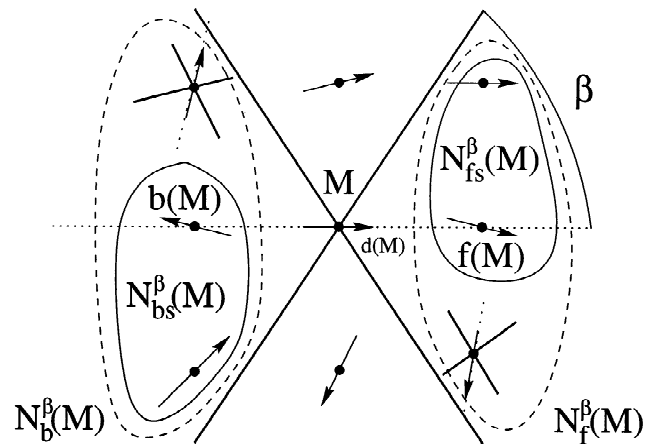


Fig. 4. 2D illustration of the construction of the neighborhoods of a site  $M$  (see text).

non-empty (see Fig. 4). Simply speaking, this symmetry constraint is related to the fact that a consistent connection implies compatible local directions. If we define the curvature criterion (see Fig. 4),

$$s(M,P) = \frac{\max^2((\vec{d}(M), \vec{u}_{MP}), (\vec{d}(P), \vec{u}_{MP}), (\vec{d}(M), \vec{d}(P)))}{\|\vec{MP}\|}, \quad (2)$$

where  $\vec{u}_{MP} = (\vec{MP}/\|\vec{MP}\|)$  and  $(\vec{u}, \vec{v})$  denotes the angle between directions  $\vec{u}$  and  $\vec{v}$ , then the definition of  $f(M)$  is (see Fig. 5)

$$f(M) = \underset{P \in \mathcal{N}_{fs}^\beta(M)}{\text{Arg min}} s(M,P). \quad (3)$$

Hence,  $f(M)$  is the best forward neighbor according to a criterion taking into account the three angles between  $\vec{d}(M)$ ,  $\vec{d}(P)$  and the direction  $\vec{MP}$  (see Fig. 5). This criterion endows the locally tracked fascicle with the lowest possible curvature. The choice of  $s(M,P)$  among other possible criteria stems from an analogy with spaghetti bending energy introduced in the next section. The best backward neighbor  $b(M)$  is defined in the same way,

$$b(M) = \underset{P \in \mathcal{N}_{bs}^\beta(M)}{\text{Arg min}} s(M,P), \quad (4)$$

where  $\mathcal{N}_{bs}^\beta(M) = \{P \in \mathcal{N}_b^\beta(M), M \in \mathcal{N}_f^\beta(P) \cup \mathcal{N}_b^\beta(P)\}$  has to be non-empty. It should be noted that forward and backward best neighbors are equivalent. Indeed orientation of  $\vec{d}(M)$  is arbitrary.

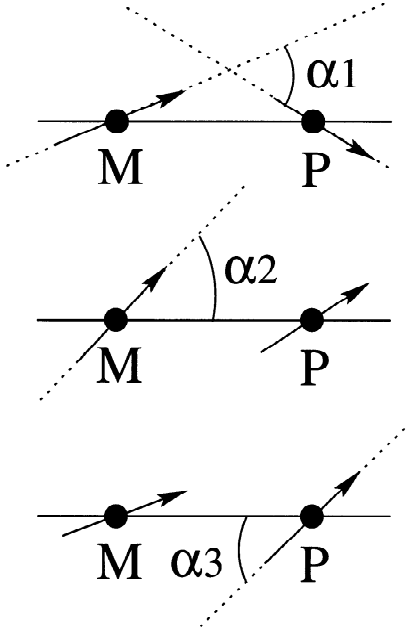


Fig. 5. The curvature criterion  $s(M,P)$  defined by Eq. (2) relies on the maximum of the angles  $\alpha_1$ ,  $\alpha_2$  and  $\alpha_3$ .

### 3.3. Fan-shaped forks

So far, each voxel has been endowed with a way of tracking forwards or backwards when compatible neighboring voxels exist. We still have to make these links bidirectional. In fact, we have to model fascicle split and merge related to the actual fiber organization or induced by the sampling of diffusion data. This is done through the creation of forks allowing the tracking to proceed further using several directions. These forks stem naturally from the definition of extended sets of linked neighbors  $\mathcal{F}(M)$  and  $\mathcal{B}(M)$  for all points of the map:

- if  $\mathcal{N}_{fs}^\beta(M) \neq \emptyset$ :

$$\mathcal{F}(M) = \{f(M)\}$$

$$\cup \{P \in \mathcal{N}_{fs}^\beta(M) \mid f(P) = M \text{ or } b(P) = M\},$$

otherwise  $\mathcal{F}(M) = \emptyset$ ;

- if  $\mathcal{N}_{bs}^\beta(M) \neq \emptyset$ :

$$\mathcal{B}(M) = \{b(M)\}$$

$$\cup \{P \in \mathcal{N}_{bs}^\beta(M) \mid f(P) = M \text{ or } b(P) = M\},$$

otherwise  $\mathcal{B}(M) = \emptyset$ .

Since these forks follow the slow direction variations embedded in best neighbor definition, they look like the standard fan-shaped split of actual fiber bundles. It should be noted that this fork definition is minimal in the sense that it results directly from the best neighbor definition. Hence, actual fibers could follow other trajectories which in our opinion cannot be reliably tracked using current DTI methods. Therefore, the tracking map made up by  $\mathcal{F}(M)$  and  $\mathcal{B}(M)$  sets aims at the inference of the more frequent trajectories, namely connections relying on numerous fibers.

This tracking map turns out to be an oriented graph whose nodes are connected by two types  $F$  and  $B$  of oriented links. The syntactic types of  $(M,P)$  oriented links stem from  $\vec{d}(M)$  orientation. These two types of links are required because according to the propagation direction of the tracking process relative to  $\vec{d}(M)$ , only one type of  $(M,P)$  links is selected to proceed further. It should be noted that the existence of the  $(M,P)$  link implies the existence of the reciprocal  $(P,M)$  link. However, syntactic types of these reciprocal links do not depend on each other but on the arbitrary orientations of  $\vec{d}(M)$  and  $\vec{d}(P)$ .

The tracking map is used to perform tracking operations according to the simple scheme illustrated by Fig. 3. Let  $\mathcal{G}$  denote the set of voxels located at the boundary of the mask  $\mathcal{W}$ . Formally, the tracking process performed from an initial input  $\mathcal{G}_{\text{input}}$  located in  $\mathcal{G}$  amounts to the construction of a sequence of  $\mathcal{W}$  subsets  $\{\mathcal{W}_0, \mathcal{W}_1, \dots, \mathcal{W}_n\}$  using the following rules:

- $\mathcal{W}_0 = \mathcal{G}_{\text{input}}$ ;
- $\mathcal{W}_1 = \{M \mid \exists M_{-1} \in \mathcal{W}_0 \text{ with } M \in \mathcal{F}(M_{-1}) \text{ or } M \in \mathcal{B}(M_{-1})\}$ ;

- for each  $i \in \{2, 3, \dots, n\}$ ,  
 $\mathcal{W}_i = \{M \mid \exists M_{-1} \in \mathcal{W}_{i-1} \text{ and } \exists M_{-2} \in \mathcal{W}_{i-2} \text{ with}$   
 $(M \in \mathcal{F}(M_{-1}) \text{ and } M_{-2} \in \mathcal{B}(M_{-1})) \text{ or}$   
 $(M \in \mathcal{B}(M_{-1}) \text{ and } M_{-2} \in \mathcal{F}(M_{-1}))\}$ .

The third rule assures that the tracking is always performed in the same direction along the underlying fascicles. Once this sequence has been computed, the answer to the brain connectivity question is the new subset  $\mathcal{G}_{\text{output}}$  defined by

$$\mathcal{G}_{\text{output}} = \mathcal{G} \cap \bigcup_{i \in \{1, 2, \dots, n\}} \mathcal{W}_i.$$

## 4. Markovian models of spaghetti plates

### 4.1. Ill-posed nature of the tracking problem

The tracking map inferred from the direction map relies on the definition of links towards best forward and backward neighbors. These links which stem from the hypothesis of slow direction variations of actual white matter fascicles are clearly dependent on errors in the direction map. Indeed a small error on  $\vec{d}(M)$  can switch the links to different neighbors. Furthermore, some errors can lead to ‘pathological’ voxels turning out to be a dead end for the tracking process (empty  $\mathcal{F}(M)$  or  $\mathcal{B}(M)$ ) although they are located inside white matter. It has to be understood that the tracking process is highly sensitive to such erroneous links or dead ends. Indeed, to be able to provide interesting information, each tracking operation requires exact links along the whole trajectory.

Unfortunately direction maps inferred from the tensor eigensystem are bound to include numerous errors. Indeed, in vivo DTI are subject to physiological noise and other motion artefacts. Furthermore, the low spatial resolution of DT images with respect to most of the fiber bundle diameters encountered in the human brain leads to significant partial volume effects. If a voxel includes several fiber directions, the tensor is less straightforward to interpret. In such situations, the main eigenvector might follow a ‘mean direction’ which may differ significantly from the directions of the underlying fascicles (Tuch et al., 1999). Therefore, tracking white matter fascicles from standard DTI data turns out to be an ill-posed problem which requires some kind of regularization (Tikhonov and Arsenin, 1977).

### 4.2. Regularization

The first level of regularization included in the construction of the tracking map is not sufficient to overcome the problem. Indeed, the slow direction variation hypothesis is used too locally to overcome large direction errors. Using longer links to overcome local gaps in the tracking trajectories could be a solution which appears rather difficult to develop in a consistent way. Furthermore, this solution would discard some important information about

the diffusion process which is lost in the eigenvector map. For instance, while the direction of the first eigenvector of a ‘flat tensor’ may largely differ from actual fiber directions, the plane defined from the two first eigenvectors is supposed to include these directions. Therefore, in our opinion, the solution has to be found at the level of the direction map computation rather than in weaknesses of the tracking process.

In the following, we propose to compute the direction map without using the tensor eigensystem. The underlying idea consists in using the slow direction variations hypothesis during the direction map inference. Hence, this approach will provide a restored direction map regularized according to the whole information included in diffusion tensor data. While the restoration will rely on local constraints on fascicle curvature like in the previous section, a global model of white matter geometry is required to allow putative fascicles to compete with each other. Performing global restoration according to local contextual constraints will lead us to introduce a Markovian random field framework (Geman and Geman, 1984).

### 4.3. Spaghetti plate analogy

The geometry of white matter illustrated by Fig. 6 is highly similar to the geometry of ‘spaghetti plates’. This analogy between fascicles and spaghetti will help us to introduce the Markovian model underlying the construction of the regularized direction map. Let us consider a single spaghetti. Before any cooking, this spaghetti can be considered as a straight line. Put in hot water, the spaghetti becomes a bended curve. The higher the water temperature is, the higher is the spaghetti curvature. A simple way to assess the cooking effect on the spaghetti geometry consists in integrating the curvature to get the spaghetti bending energy  $E$ ,

$$E(\text{spaghetti}) = \int_0^{\text{length}} \frac{\mathcal{K}}{2} c^2(s) ds, \quad (5)$$

where  $s$  is simply a curvilinear abscissa along the spaghetti,  $c(s)$  is the spaghetti curvature at abscissa  $s$  and  $\mathcal{K}$  is the stress rigidity. This energy, well known in chemistry as the Kratky-Porod model of semi-flexible polymers (Chaikin and Lubensky, 1995), can be extended in a straightforward way to a whole spaghetti plate. The tracking algorithm introduced in the previous section is searching locally for the fascicle with the lowest curvature. This local point of view is not robust to noise in the direction map. This weakness can be overcome if a global point of view is chosen: searching for the fascicle set which realizes the best trade-off between diffusion data and a low bending energy constraint.

The computation of the regularized direction map can be classically interpreted in a Bayesian framework. The

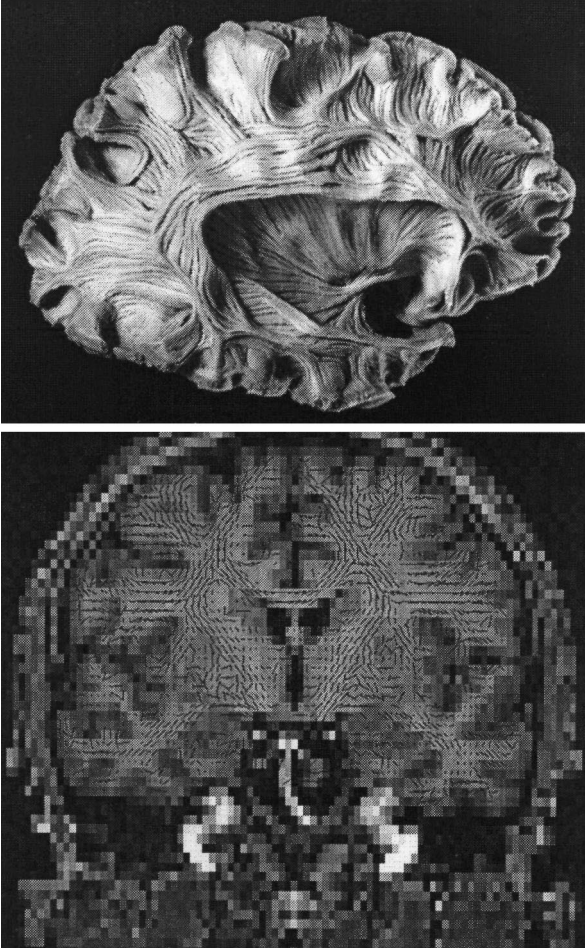


Fig. 6. (Upper) The spaghetti plate like geometry of white matter illustrated by a brain dissection (The Virtual Hospital, University of Iowa); (lower) first eigenvector of the diffusion tensor superimposed on the corresponding T1-weighted slice.

optimal direction map  $D_{\text{opt}}$  has to maximize the a posteriori probability  $p(D/T)$ , where  $T$  denotes the diffusion tensor data and  $D$  denotes a random field which covers all possible direction maps. Bayes rule allows us to introduce the a priori knowledge on the low curvature of fascicles,

$$p(D/T) = \frac{p(T/D) \cdot p(D)}{p(T)}. \quad (6)$$

Since  $p(T)$  does not depend on  $D$ , maximizing  $p(D/T)$  amounts to maximizing the product  $p(T/D) \cdot p(D)$ . In the following, we propose a model of these two probabilities which allows the computation of  $D_{\text{opt}}$ . The a priori probability  $p(D)$  will be related to the bending energy of the equivalent spaghetti plate in order to favor low curvature fascicles. The a posteriori probability  $p(T/D)$  will be related to the nature of water diffusion in white matter: for each voxel  $M$ , the diffusion coefficient in the direction  $\vec{d}(M)$  should be as high as possible. It should be noted that if  $p(D)$  is the uniform probability density,  $D_{\text{opt}}$

turns out to be the map made up by the tensor principal eigenvectors.

#### 4.4. A priori models

This subsection is concerned with the design of a distribution modeling the a priori probability  $p(D)$ . This distribution should endow spaghetti plate like realizations with a high probability related to the underlying bending energy. The realization of the random variables  $\vec{d}(M)$  of the field  $D$  are unitary vectors with any 3D direction. Let us consider a voxel  $M$ . This voxel has to belong to one fascicle. Let  $\vec{d}(M)$  denote the putative local direction of this fascicle for a realization of the field. Since fascicles cannot end up inside white matter, we have to find neighboring voxels, forwards and backwards, with similar fascicle directions (or perhaps the boundary of white matter). Moreover, this property is sufficient to define the whole geometry of a plausible fascicle set. Mathematically speaking, this property means that  $p(\vec{d}(M))$  depends only on the realizations of the fascicle directions of  $M$  neighbors. Therefore, this random field is Markovian which is very interesting from a practical point of view because if the positivity condition is respected (each field realization is endowed with a non-zero probability), the global field probability  $p(D)$  follows a Gibbs distribution (Geman and Geman, 1984):

$$p(D) = \frac{1}{Z^S} e^{-\sum_c V_c^S}, \quad (7)$$

where  $Z^S$  is a normalizing constant and  $V_c^S$  are potential functions defined on interaction cliques. These interaction cliques are subsets of random variables of the field which interact with each other. Each clique  $c$  is endowed with a potential function in which the nature of this interaction is embedded. Intuitively, the lower the potential is, the higher is the probability of the clique realization. It should be noted that one random variable usually belongs to several cliques. Summing all these potential functions leads to the global energy of the field which is minimal for the realizations with the highest probability.

Considering the nature of the field interactions, a straightforward choice for the clique system is  $\{M \cup (\mathcal{N}_{26}^c(M) \cap \mathcal{W}), M \in \mathcal{W}\}$ , where  $\mathcal{N}_{26}^c(M)$  denotes  $M$  26-neighborhood. The choice of interaction potentials is more difficult because various functions could lead to spaghetti plate like deep local minima for the underlying global energy (Poupon et al., 1998a). The analogy with spaghetti will lead us to build this potential on an equivalent of the spaghetti local bending energy (cf. Eq. (7)) which is not so easy to define considering the fascicle sampling (see Eq. (2)).

An interesting question is related to the number of neighbor directions to be implied in the potential. Indeed, if  $\vec{d}(M)$  is supposed to give the local fascicle direction,

several neighboring fascicles belonging to the same bundle usually follow a similar direction (see Fig. 6). Then, to keep with our analogy, the question is the following: is it possible to find a model giving a highest probability to an ill-cooked spaghetti plate where a lot of the spaghetti are stuck together in large bundles compared with a plate endowed with equal bending energy but evenly stirred during cooking in order to split the bundles?

To investigate this question, we realized the following experiment. Let us consider that all  $P \in \mathcal{N}_f^\beta(M)$  (respectively  $P \in \mathcal{N}_b^\beta(M)$ ) have been sorted out according to increasing magnitude of  $(\vec{d}(M), \vec{d}(P))$  angle (see Fig. 4). Then, let  $\mathcal{N}_f^{\beta,k}(M)$  (respectively  $\mathcal{N}_b^{\beta,k}(M)$ ) denote the subset made up of the  $k$  first neighbors. To deal with border voxels, we set  $\mathcal{N}_f^{\beta,k}(M) = \mathcal{N}_f^\beta(M)$  (respectively  $\mathcal{N}_b^{\beta,k}(M) = \mathcal{N}_b^\beta(M)$ ) when  $\mathcal{N}_f^\beta(M)$  (respectively  $\mathcal{N}_b^\beta(M)$ ) contains less than  $k$  points. A three-parameter model family can be defined from the following potential functions:

$$V_S^{\beta,k,\theta}(M,D) = \sum_{P \in \mathcal{N}_f^{\beta,k}(M) \cup \mathcal{N}_b^{\beta,k}(M)} \Phi_\theta((\vec{d}(M), \vec{d}(P))), \quad (8)$$

where  $\Phi_\theta(\alpha) = \alpha^2 / (\theta^2 + \alpha^2)$  is used rather than a quad-

atic penalty term to reduce over-regularization problems at the level of bundle edges (Meer et al., 1991; Poupon et al., 1998a). In order to study the geometry of high probability configurations,  $U_S^{\beta,k,\theta} = \sum_{\mathcal{D}} V_S^{\beta,k,\theta}(M,D)$  is minimized from a random cubic direction map using an ICM like deterministic algorithm (Besag, 1986). The resulting direction map is then transformed in a tracking map according to the previous section method and a few tracking operations are performed. Some results presented in Fig. 7 show that large values of  $k$  favour thick bundles as expected.

Simulated and real regularization experiments performed with this type of models and some variants have proved their efficiency to recover the organization of large bundles (see Fig. 8). However, potential over-regularization problems with models using several neighbors (Poupon et al., 1998a) have led us to investigate further one-neighbor models. Indeed, our connectivity mapping aim implies that regularization preserves as far as possible thin bundles.

Although tracking operations performed with local minima related to the previous one-neighbor models reveal some long fascicle like trajectories (see Fig. 7), these direction maps turn out to contain numerous dead ends for

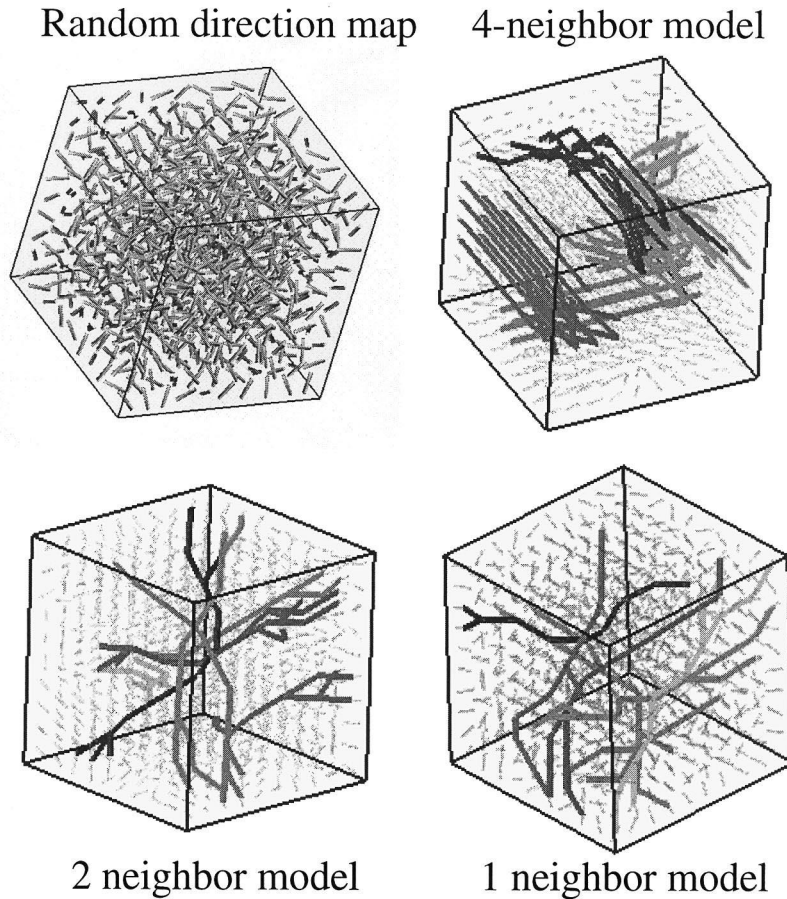


Fig. 7. Geometry of some high probability configurations obtained from a cubic random direction map after deterministic minimization. The underlying spaghetti plate models are defined from Eq. (8) potential family with  $\beta = 45^\circ$ ,  $\alpha = 10^\circ$  and different values of  $k$ . The results of some tracking operations are highlighted to show that large values of  $k$  favour thick bundles of aligned fascicles.

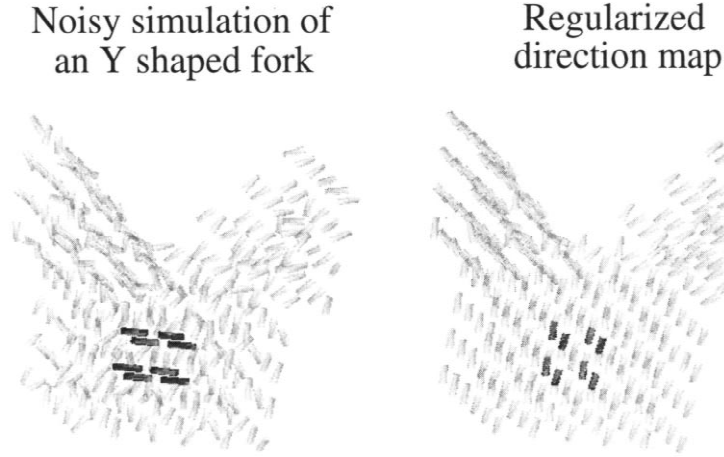


Fig. 8. Regularization of a simulated Y-shaped fork using a model related to Eq. (8) potential with four neighbors. Orientations of simulated anisotropic diffusion tensors have been highly corrupted and a cube of eight tracking dead ends have been added in the middle of the bundle (cf. Poupon et al., 1998a).

the tracking process. This problem results from the fact that  $V_s^{\beta,k,\theta}(M,D)$  potential do not take into account  $\vec{MP}$  directions. Indeed, with  $k > 1$ , the fascicle trajectories embedded in this potential are not really known. Because of this weakness, the one-neighbor model gives high probability to absurd direction maps, for instance a check-board where black squares have horizontal directions and white squares have vertical directions. Therefore, we designed a new potential which stems directly from the tracking algorithm curvature criterion (see Eq. (2)),

$$V_s(M,D) = s(M,f^{90}(M)) + s(M,b^{90}(M)), \quad (9)$$

where  $f^{90}(M)$  and  $b^{90}(M)$  are best linked neighbors related to half-cones with  $\beta=90^\circ$  aperture angle, that cover the whole 26-neighborhood. While  $s(M,P)$  curvature criterion only mimics the spaghetti local bending energy (Eq. (5)), because of the discrete nature of the direction map, it is supposed to lead to a global energy of similar landscape. We studied the geometry of this model local minima with the same experiment than before (see Fig. 9). The corresponding direction maps turn out to be almost dead end free.

#### 4.5. Regularized direction map

In this subsection, we propose a model of  $p(T/D)$  which is combined with the a priori model of Eq. (9) to define the optimal direction map.

Let us assume now that the tensor measurement in one voxel  $M$  depends only on  $\vec{d}(M)$ . This rather reasonable hypothesis will lead to a second Gibbs distribution corresponding to a field without interaction. The conditional probability  $p(T/D)$  can be rewritten in the following way:

$$p(T/D) = \prod_M p(T(M)/\vec{d}(M)).$$

Assuming first that knowing a local fascicle direction

$\vec{d}(M)$ , any tensor measurement  $T(M)$  has a non-zero probability, and second that the tensor measurement probability distribution  $p(T(M)/\vec{d}(M))$  has stationary properties throughout the VOI,  $p(T/D)$  can be rewritten as

$$\begin{aligned} p(T/D) &= \frac{1}{Z^T} \prod_M e^{-v_T^M(\vec{d}(M))} = \frac{1}{Z^T} e^{-\sum_M v_T^M(\vec{d}(M))} \\ &= \frac{1}{Z^T} e^{-\sum_M v_T(T(M),\vec{d}(M))}, \end{aligned}$$

where  $Z^T$  is a normalizing constant. Finally, in order to get a probability  $p(T(M)/\vec{d}(M))$  decreasing with the dis-

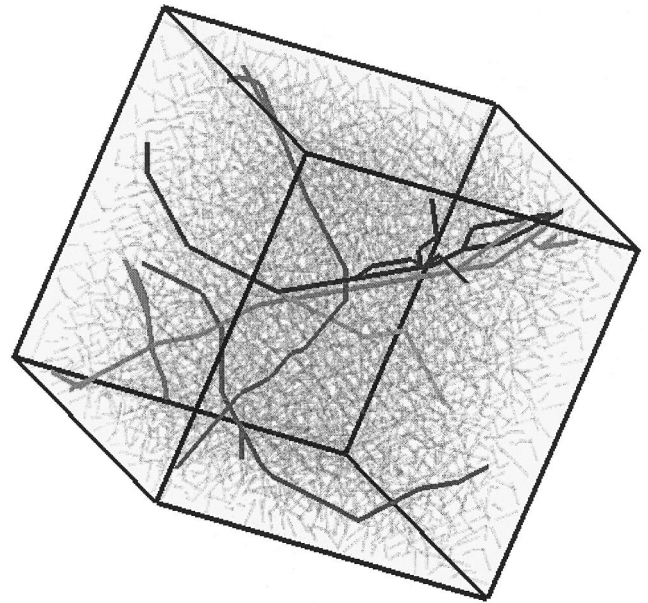


Fig. 9. Geometry of a high probability configuration obtained from a cubic random direction map after deterministic minimization. The underlying one-neighbor spaghetti plate model is defined from Eq. (9). Most of the tracking operations performed from a random voxel reach two faces of the cubic map.

crepancy between diffusion in the direction  $\vec{d}(M)$  and the diffusion in the direction of the tensor first eigenvector  $\vec{e}_1(M)$ , we propose to use the following potential function:

$$V_T(T(M), \vec{d}(M)) = \left( \frac{\vec{d}(M)'T(M)\vec{d}(M) - \overrightarrow{e_1(M)'T(M)e_1(M)}}{\|T(M)\|} \right)^2 \quad (10)$$

The discrepancy is normalized by the tensor norm (Basser and Pierpaoli, 1996) in order to remove all diffusion-based information apart from anisotropy.

Combining all the previous equations leads to the expression of  $p(D/T)$  which turns out to be a new Gibbs distribution where the additional cliques relative to Eq. (7) are the trivial ones, namely the singletons  $\{M\}$ . This new distribution leads now to the definition of  $D_{opt}$  as the direction map which minimizes the energy  $U(D)$  given by

$$U(D) = \alpha U_s(D) + U_T(D) \\ = \alpha \sum_M V_s(M, D) + \sum_M V_T(T(M), \vec{d}(M)). \quad (11)$$

Finally, this new definition clearly shows that the optimal direction map  $D_{opt}$  is a trade-off between the measured tensor data and the a priori knowledge on the low curvature of fascicles. The constant  $\alpha$  reflects the influence of this a priori knowledge.

### 5. Results

All the results described in the following stem from deterministic minimization of  $U(D)$  (cf. Eq. (11)). The

state space of the random variables  $\vec{d}(M)$  has been discretized in 162 uniformly distributed directions. An ICM like algorithm is used to get the minimum the nearest to the  $\vec{e}_1(M)$  direction map (Besag, 1986). The computation time is about 1 hour on a conventional workstation. Further work is required to assess the interest of using stochastic minimization.

#### 5.1. Influence of the a priori model weight

Regularization of one set of real data has been performed with eleven different values of the weighting parameter  $\alpha$ . Then, in order to study the influence of regularization on the tracking map topology, several subsets of points have been defined from the construction of  $\mathcal{F}(M)$  and  $\mathcal{B}(M)$  extended neighborhoods ( $\beta = 45^\circ$ ). It should be noted that the  $90^\circ$  cone aperture is only used during regularization in order to penalize the worst configurations. However, during a tracking operation, the aperture angle is largely reduced in order to forbid anatomically meaningless links. The evolution relative to  $\alpha$  of the cardinals of four specific sets of points has been studied (see Fig. 10):

*Fascicle nodes*: sites endowed with exactly one forward neighbor and one backward neighbor ( $\mathcal{B}(M) = \{b(M)\}$  and  $\mathcal{F}(M) = \{f(M)\}$ );

*Junctions*: sites related to the merge (or split) of several fascicles made up of points of the previous type ( $\text{cardinal}(\mathcal{B}(M)) \times \text{cardinal}(\mathcal{F}(M)) > 1$ );

*Gate to gray matter*: sites leading to gray matter ( $N_f^{45}(M) = \emptyset$  or  $N_b^{45}(M) = \emptyset$ );

*Pathological sites*: sites endowed with forward (or

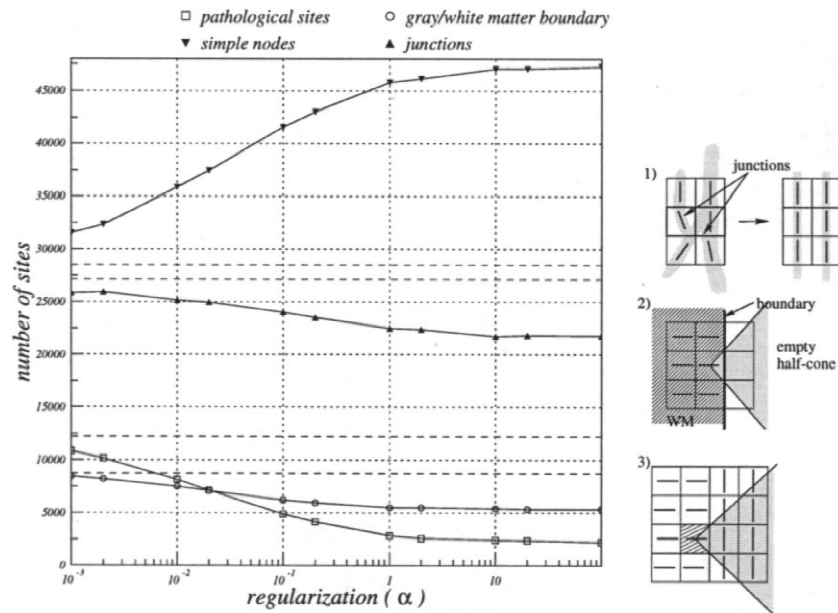


Fig. 10. (Left) Evolution of the numbers of four different types of configurations. (Right) (1) fascicle mixing inside a bundle before regularization versus a bunch of aligned fascicles after regularization; (2) sites of white matter leading to gray matter; (3) pathological site without tracking possibility.

backward) basic neighbors, but no forward (or backward) symmetrical neighbors, i.e., pathological sites ( $(N_{fs}^{45}(M) = \emptyset \text{ and } N_{fs}^{45}(M) \neq \emptyset)$  or  $(N_{bs}^{45}(M) = \emptyset \text{ and } N_{bs}^{45}(M) \neq \emptyset)$ ).

Fig. 10 presents the evolution from no regularization (left asymptotes) to high regularization (right). First, the number of pathological sites (see Fig. 10(3)) decreases dramatically with the regularization which demonstrates the efficiency of the model. Second, the regularization leads to a decrease of the number of junctions and to a dramatic increase of the number of simple fascicle nodes. This effect is mainly due to a reorganization of the fascicles inside larger bundles (see Fig. 10(1)) which corresponds to the usual underlying anatomical reality. Indeed, the chronotopic establishment of the connections leads to topographically ordered bundles (Molnár, 1998). Hence, the large bundles are endowed with somatotopic organizations, which means that different parts of the

bundle section include axons connecting different brain areas. Finally, the number of sites leading to gray matter decreases slightly which is related to the fact that with a  $90^\circ$  cone aperture during the regularization, only convex areas of the boundary (see Fig. 10(2)), namely cortical gyri, are not penalized. While these areas are the main cortical connexion locations, this effect calls for refinements of the regularizing model. All the curve evolutions reach limits beyond which no more topological effect is observed on the fascicle set. This observation suggests that the weight  $\alpha = 1$  is a reasonable trade-off between regularization and fidelity to the data which has been used for further experiments.

### 5.2. Trajectory restoration

Other experiments have been performed to compare the

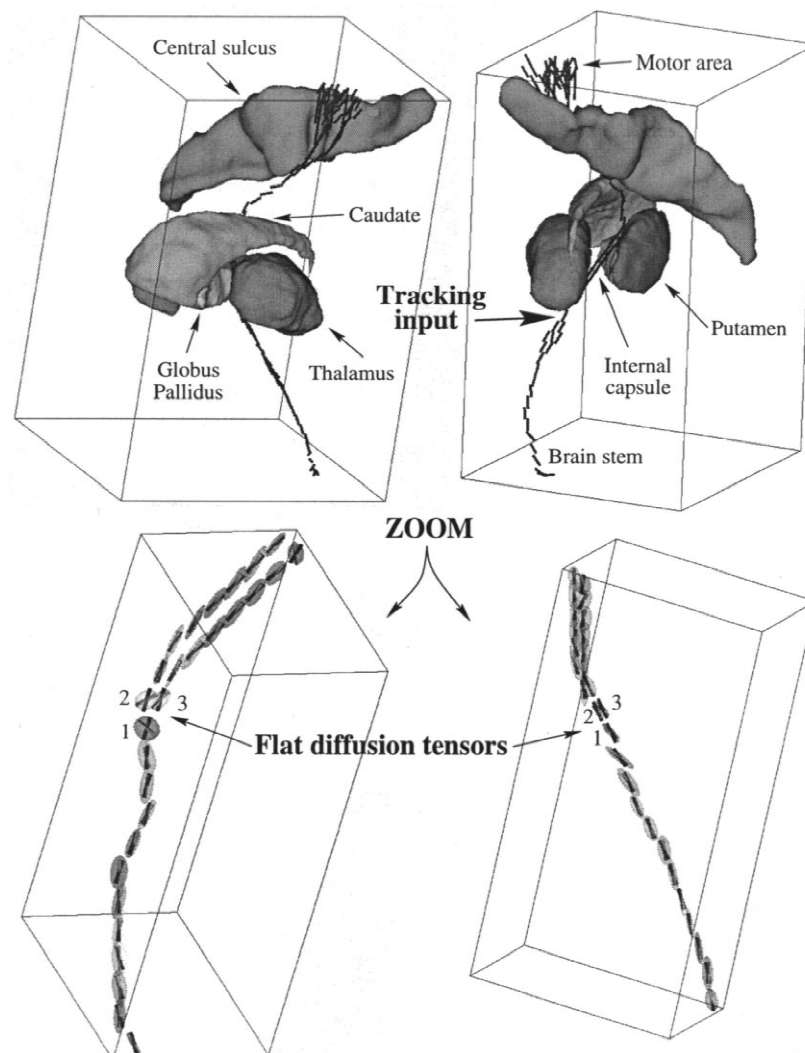


Fig. 11. (Upper) Tracking of putative trajectories of pyramidal fibers from motor area until brain stem. (Lower) A zoom on the trajectory to visualized regularization effects. Tensor first eigen vectors are represented by a light cylinder while regularized directions appear as a dark cylinder. Tensors are represented by ellipsoids. The largest direction corrections are performed for flat tensors endowed with two high eigenvalues. These tensors are supposed to correspond to fiber crossings or fan-shaped forks.

tracking process behaviours with and without regularization. Two kinds of problems occur before regularization. While the tracking process highlights some plausible fiber trajectories, these trajectories are usually mixed with very unplausible ones because of a few misoriented local directions. Moreover, the tracking process which should follow thin fascicles often invades the whole surrounding

bundle (Poupon et al., 1999). The second kind of problems is related to the presence of numerous dead ends in the middle of white matter which stop the tracking process. All these problems are largely minimized when using the regularized tracking map. Unfortunately, validation relative to actual anatomical connectivity, which is currently not available, would be required for further comparison. The

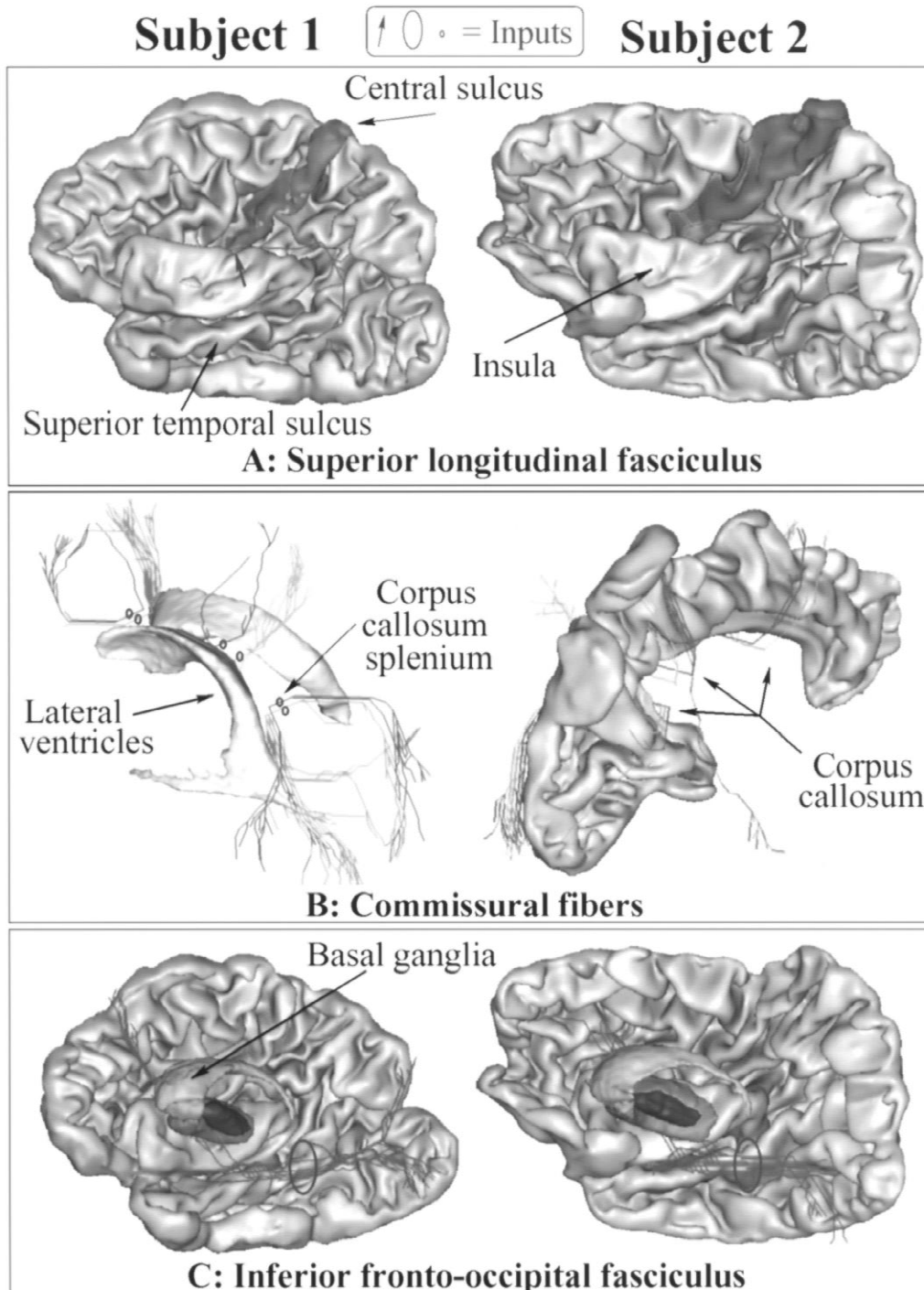


Fig. 12. Examples of tracking from one single input voxel (A,B) or from small sets of neighboring voxels endowed with similar putative fiber orientations (as observed in 2D slices with superimposed directions) (C). In most of the images the cortex is visualised from below after a virtual split.

regularization effect is illustrated in Fig. 11 for a putative fiber trajectory included in the pyramidal pathway. This pathway drives motor impulse from motor areas to brain stem. Before regularization the tracking is stopped at the level of flat tensors whose first eigenvectors are meaningless. These directions have been rotated in the high diffusion plane by the regularization process in order to create a consistent slow direction variation trajectory.

### 5.3. Tracking experiments

Finally, various tracking experiments have been performed according to the scheme proposed in Fig. 3 or to a similar one for which the input is located inside white matter. Some of these experiments were aimed at tracking the putative trajectories of short and long association fibers (cf. Fig. 12(A,C)). Other experiments were aimed at tracking the putative trajectories of commissural fibers (cf. Fig. 12(B)) and projection fibers (cf. Fig. 11). All these experiments led to low curvature trajectories in accordance with the a priori knowledge injected in the regularization process. Most of these trajectories were endowed with fan-shaped terminations and a few forks compatible with the actual organization of white matter. While no real validation is currently available, some of these tracking experiments revealed trajectories akin to well-known white matter bundles described in the anatomical literature (Dejerine, 1895): pyramidal tracts (cf. Fig. 11), superior longitudinal fasciculus (cf. Fig. 12(A)), occipito-frontal fasciculus (cf. Fig. 12(C)), occipito-occipital commissural axons crossing corpus callosum splenium (cf. Fig. 12(B)).

## 6. Discussion and conclusion

Mapping the living human brain connectivity with clinical scanners and reasonable acquisition times is a difficult challenge. Indeed, fascicle tracking is a mathematically ill-posed problem especially sensitive to noise in the direction map inferred from the DTI data. For instance, each error in the direction map can lead to a random fork in the tracking process without underlying anatomical meaning. Furthermore, the typical spatial resolution of echo planar images results in partial volume effects mixing the fascicle directions while attempts to achieve higher resolution reduces SNR and generally leads to more severe image artefacts.

A straightforward way to reduce the sensitivity to noise consists in increasing acquisition time to improve SNR (Conturo et al., 1999). Unfortunately this approach does not address problems induced by partial volume effect and is not compatible with clinical constraints. In our opinion, the difficulties related to the ill-posed nature of the tracking problem can be overcome by the introduction of a

priori knowledge on the white matter geometry. In this paper, we have shown that such an approach leads to improvements in DTI-based fascicle tracking. While the regularization method proposed in this paper may appear rather intricate compared to more usual image smoothing approaches, it should be noted that the underlying idea is a restoration preserving as far as possible the DTI spatial resolution. Indeed, considering the current spatial resolution of in vivo DTI (2 mm), preserving this resolution is crucial for the tracking of thin cortico-cortical bundles which are of high interest in neuroscience. For instance, Gaussian smoothing of the tensor data, which has been recently proposed as a preprocessing to tracking (Westin et al., 1999), removes information on thin bundles. An alternative consisting in applying simulated anisotropic diffusion on raw diffusion-weighted images has been proposed recently to overcome problems related to negative eigenvalues in the tensor (Parker et al., 1999). This method, which prevents smoothing across edges, preserves macroscopic anatomical information like the boundary between brain and CSF. However this approach is bound to increase partial volume effects inside white matter. Nevertheless, the design of an anisotropic diffusion scheme based on ‘edges’ computed from tensor orientations could be an interesting alternative to our Markovian framework.

In summary, we have introduced a sequence of robust algorithms allowing the tracking of white matter fascicles using DTI. A number of these algorithms are completely new: eddy current distortion correction using mutual information, robust regression to assess the diffusion tensor, computation of a regularized direction map from DTI data and, finally, a fascicle tracking algorithm dealing with fascicle junctions. A number of questions related to some of the parameters of our method remain open: the weight of a priori knowledge, the choice of the potential functions, the neighborhood cone aperture, the minimization algorithm. Furthermore, some refinements are required to get rid of the bias induced by grid effects. An important future direction of research consists in improving the angular resolution of the diffusion data in order to deal with fascicles crossing inside a voxel (Tuch et al., 1999). Addressing these points in a consistent way would require knowledge of a gold standard with which to test the validity and accuracy of the methods. Therefore one of the challenges to take up rapidly is the design of reliable validation approaches using for instance animals and standard tracer-based methods.

This paper outlines the opening of a new research domain for the image analysis community. Indeed, dealing with tensor images calls for the development of completely new algorithms. This direction of research could lead to the first method giving access in vivo to the human brain connectivity. Such a method would have a great impact both on brain mapping and on pathological studies.

## References

- Basser, P., Pierpaoli, C., 1996. Microstructural and physiological features of tissues elucidated by quantitative-diffusion-tensor MRI. *J. Magn. Reson.* 111, 209–219.
- Basser, P., Pierpaoli, C., 1998. A simplified method to measure the diffusion tensor from seven MR images. *J. Magn. Reson. Med.* 39, 928–934.
- Basser, P., Mattiello, J., LeBihan, D., 1994a. Estimation of the effective self-diffusion tensor from the NMR spin echo. *J. Magn. Reson.* 103, 247–254.
- Basser, P., Mattiello, J., LeBihan, D., 1994b. MR diffusion tensor spectroscopy and imaging. *Biophys. J.* 66, 259–267.
- Besag, J., 1986. On the statistical analysis of dirty pictures. *J. R. Statist. Soc. Ser. B (Methodol.)* 48 (3), 259–302.
- Chaikin, P., Lubensky, T., 1995. In: *Principles of Condensed Matter Physics*. Cambridge University Press, Cambridge.
- Conturo, T.E., Lori, N.F., Cull, T.S., Akbudak, E., Snyder, A.Z., Shimony, J.S., McKinstry, R.C., Burton, H., Raichle, M.E., 1999. Tracking neuronal fiber pathways in the living human brain. *Proc. Natl. Acad. Sci. USA* 96, 10422–10427.
- Dejerine, J., 1895. *Anatomie Des Centres Nerveux*. Rueff, Paris.
- Fox, P.T., Perlmutter, L.S., Raichle, M.E., 1985. A stereotactic method of anatomical localization for positron emission tomography. *J. Comput. Assist. Tomogr.* 9, 141–153.
- Geman, S., Geman, D., 1984. Stochastic relaxation, Gibbs distributions, and the bayesian restoration of images. *IEEE Trans. Pattern Anal. Machine Intelligence PAMI-6* (6), 721–741.
- Haselgrove, J.C., Moore, J.R., 1996. Correction for distortion of echo-planar images used to calculate the apparent diffusion coefficient. *Magnetic Resonance in Medicine* 36, 960–964.
- Jones, D.K., Simmons, A., Williams, S.C.R., Horsfield, M.A., 1999. Non-invasive assessment of axonal fiber connectivity in the human brain via diffusion tensor MRI. *Magn. Reson. Med.* 42, 37–41.
- Le Bihan, D., 1995. In: *Diffusion and Perfusion Magnetic Resonance Imaging*. Raven Press, New York.
- Lohman, G., Von Cramon, D.Y., 1998. Automatic detection and labelling of the human cortical folds in magnetic resonance data sets. In: *ECCV'98*, Freiburg.
- Mangin, J.-F., Frouin, V., Bloch, I., Régis, J., Lopez-Krahe, J., 1995. From 3D magnetic resonance images to structural representations of the cortex topography using g topology preserving deformations. *J. Math. Imaging Vision* 5 (4), 297.
- Mangin, J.-F., Régis, J., Frouin, V., 1996. Shape bottlenecks and conservative flow systems. In: Press, I.C.S. (Ed.), *IEEE/SIAM Proc. of the MMBIA*, San Francisco, CA, pp. 319–328.
- Mangin, J.-F., Coulon, O., Frouin, V., 1998. Robust brain segmentation using histogram scale-space analysis and mathematical morphology. In: *MICCAI'98*, MIT, LNCS-1496. Springer, Berlin, pp. 1230–1241.
- Meer, P., Mintz, D., Rosenfeld, A., Kim, D.Y., 1991. Robust regression methods for computer vision: a review. *Int. J. Comput. Vis.* 6, 59–70.
- Miller, M., Christensen, G., Amit, Y., Grenander, U., 1993. A mathematical textbook of deformable neuroanatomies. *Proc. Natl. Acad. Sci. USA* 90, 11944–11948.
- Molnár, Z., 1998. In: *Development of Thalamocortical Connections*. Springer, Berlin.
- Mori, S., Crain, B., Chacko, V.P., van Zijl, P.C.M., 1999. Three dimensional tracking of axonal projections in the brain by magnetic resonance imaging. *Ann. Neurol.* 45, 265–269.
- Naf, M., Kubler, O., Kikinis, R., Shenton, M., Szekely, G., 1996. Characterization and recognition of 3D organ shape in medical image analysis using skeletonization. In: Press, I.C.S. (Ed.), *IEEE/SIAM Proc. of the MMBIA*, San Francisco, CA, pp. 139–150.
- Parker, G.J.M., Werring, D.J., Schnabel, J.A., Symms, M.R., Barker, G.J., 1999. Noise reduction in diffusion tensor imaging-reducing systematic anisotropy errors. In: *VIIth ISMRM*, Philadelphia, PA, USA, p. 1798.
- Poupon, C., Mangin, J.-F., Frouin, V., Régis, J., Poupon, F., Pachot-Clouard, M., LeBihan, D., Bloch, I., 1998a. Regularization of MR diffusion tensor maps for tracking brain white matter bundles. In: *MICCAI'98*, MIT, LNCS-1496. Springer, Berlin, pp. 489–498.
- Poupon, F., Mangin, J.-F., Hasboun, D., Poupon, C., Magnin, I., Frouin, V., 1998b. Multi-object deformable templates dedicated to the segmentation of brain deep structures. In: *MICCAI'98*, MIT, LNCS-1496. Springer, Berlin, pp. 1134–1143.
- Poupon, C., Clark, C.A., Frouin, V., LeBihan, D., Bloch, I., Mangin, J.-F., 1999. Inferring the brain connectivity from MR diffusion tensor data. In: *MICCAI'99*, Cambridge, UK, LNCS-1679. Springer, Berlin, pp. 453–462.
- Régis, J., Mangin, J.-F., Frouin, V., Sastre, F., Peragut, J.C., Samson, Y., 1995. Generic model for the localization of the cerebral cortex and preoperative multimodal integration in epilepsy surgery. *Stereotact. Funct. Neurosurg.* 65, 72–80.
- Roland, P.E., Zilles, K., 1994. Brain atlases: a new research tool. *Trends Neurosci.* 17, 458–467.
- Talairach, J., Szikla, G., Tournoux, P., Prossalenti, A., Bordas-Ferrer, M., Covelto, L., Iacob, M., Mempel, E., 1967. In: *Atlas d'Anatomie Stéréotaxique du Téleencéphale: études Anatomoradiologiques*. Masson et Cie, Paris.
- Thirion, J.-P., 1998. Image matching as a diffusion process: an analogy with Maxwell's demons. *Medical Image Analysis* 2, 243–260.
- Thompson, P., Schwartz, C., Toga, A., 1996. High-resolution random mesh algorithms for creating a probabilistic 3d surface atlas of the human brain. *Neuroimage* 3, 19–34.
- Tikhonov, A.N., Arsenin, V.Y., 1977. In: *Solution of Ill-posed Problems*. Winston, New York.
- Tuch, D.S., Weisskoff, R.M., Belliveau, J.W., Wedeen, V.J., 1999. High angular resolution diffusion imaging of the human brain. In: *VIIIth ISMRM*, Philadelphia, PA, USA.
- Wells III, W.M., Viola, P.A., Atsumi, H., Najajima, S., Kikinis, R., 1997. Multi-modal volume registration by maximization of mutual information. *Medical Image Analysis* 1 (1), 35–51.
- Westin, C.-F., Maier, S., Khidir, B., Everett, P., Jolesz, F.A., Kikinis, R., 1999. Image processing for diffusion tensor magnetic resonance imaging. In: *MICCAI'99*, Cambridge, UK, LNCS-1679. Springer, Berlin, pp. 441–452.
- Young, M., Scannell, J., Burns, G., 1995. In: *The Analysis of Cortical Connectivity*. Neuroscience Intelligence Unit, Springer, Berlin.